



CHORUS

This is the accepted manuscript made available via CHORUS. The article has been published as:

Minimal model of directed cell motility on patterned substrates

Matthew S. Mizuhara, Leonid Berlyand, and Igor S. Aranson

Phys. Rev. E **96**, 052408 — Published 15 November 2017

DOI: [10.1103/PhysRevE.96.052408](https://doi.org/10.1103/PhysRevE.96.052408)

Minimal model of directed cell motility on patterned substrates

Matthew S. Mizuhara,^{1,*} Leonid Berlyand,^{2,†} and Igor S. Aranson^{3,‡}

¹*Department of Mathematics and Statistics, The College of New Jersey, Ewing, NJ 08628, USA.*

²*Department of Mathematics, Pennsylvania State University, University Park, PA 16802, USA.*

³*Departments of Biomedical Engineering, Chemistry and Mathematics, Pennsylvania State University, University Park, PA 16802, USA.*

Crawling cell motility is vital to many biological processes such as wound healing and the immune response. Using a minimal model we investigate the effects of patterned substrate adhesiveness and biophysical cell parameters on the direction of cell motion. We show that cells with low adhesion site formation rates may move perpendicular to adhesive stripes while a those with high adhesion site formation rates results in motility only parallel to the substrate stripes. We explore the effects of varying the substrate pattern geometry and the strength of actin polymerization on the directionality of the crawling cell. These results reveal that high strength of actin polymerization results in motion perpendicular to substrate stripes only when the substrate is relatively non-adhesive; in particular this suggests potential applications in motile cell sorting and guiding on engineered substrates.

I. INTRODUCTION

Eukaryotic cell motility is crucial to many biological processes ranging from wound healing [1] and the immune response [2] to cancer metastasis [3]. The underlying biophysical mechanisms leading to persistent cell motion are generally understood: actin treadmilling (polymerization) drives protrusions at the cell front [4, 5] while adhesion complexes transfer traction forces to the substrate [6] and myosin motors produce contractions at the cell rear [7, 8]. However the interactions of these mechanisms with external stimuli, e.g., varying substrate properties, remains relatively unexplored.

Prototypical cells for experiments, and subsequently, mathematical models, are keratocytes (e.g., harvested from fish scales). In homogeneous environments, once individual keratocytes initiate motion they exhibit characteristic crescent profiles and maintain essentially constant shape, speed, and direction [9, 10]. Moreover as the characteristic cell length/width is two orders of magnitude larger than the height while motile, keratocytes are amenable to 2D models and thus may be considered the simplest cells for development of mathematical models (however there are additionally recent advances in 3D modeling techniques [11]).

For a general overview of both biological aspects of actin driven cell motility and of several modeling approaches we recommend the survey [12]. In particular, in recent years both free boundary and phase-field models have been extremely successful in replicating, explaining, and predicting experimental results (e.g., [13–19]), see for review [20]. We highlight that recent mathematical analyses have elucidated biological mechanisms [21–24], and numerical simulations have described a wide range of behaviors ranging from motility initiation via stochastic

fluctuations [25] to capturing various modes of motility such as stick-slip and bipedal motions [26–28].

The focus of our study is the effect of variable substrate properties on the direction of the cell’s motion. In experimental settings the substrate may be coated non-homogeneously with fibronectins which allow for the creation of adhesion complexes, resulting in regions of variable adhesiveness. In [29] microcontact printing of regions enriched with (or depleted of) fibronectins resulted in alternating substrate stripes of high and low adhesiveness with period smaller than the cell size. In this setting the authors in [29] found that keratocytes exhibited directed motion parallel to the adhesive stripes. Similar results exhibiting directed motion parallel to substrate stripes were also obtained in [30, 31] for fibroblast cells.

We briefly mention other works which study the effect of non-homogeneous substrates. If the cell’s size is smaller than the width of the adhesive stripe then both experiment and modeling [28, 32] observe that the cell may be contained within adhesive regions: when the cell encounters a region of low adhesiveness it will change its direction in order to remain on regions of high adhesiveness. Moreover, it has been observed that cell morphologies can be controlled when placed on specific adhesive geometries [33, 34] and directionality can be controlled on substrates with varying stiffness and micropatterning [34–37]. As such, controlling and predicting the motility of keratocytes on engineered patterned substrates has direct applications to cell screening and sorting both in biomimetics [38] and experimental settings.

In this work we study the directionality of a motile cell on a patterned substrate with alternating stripes of high and low adhesiveness; here the cell size is assumed to be larger than the stripe width so that the cell spans several regions of both high and low adhesion, corresponding to the experimental setup of [29]. We stress that the dynamics of adhesion site formation are, in general, complex [39–42]. In [28] a phase-field model which included both dynamics of the adhesion site formation as well as substrate deformation (e.g., due to traction forces generated by the cell) was introduced. The authors in-

* mizuharm@tcnj.edu

† lvb2@psu.edu

‡ isa12@psu.edu; Corresponding author

roduced patterned adhesiveness and reproduced the experimental results observed in [29] wherein cells moved parallel to substrate stripes. The existence and stability of such parallel motions were explained via analysis of a simplified system of (ordinary) differential equations (cf. system (1)-(5)). Surprisingly, in [28] it was also obtained for certain parameter regimes that the cells move perpendicular (rather than parallel) to substrate adhesion stripes. More specifically, when the attachment rate of adhesion complexes is sufficiently high (e.g., adhesive parts of stripes have high adhesiveness), numerical simulations reproduce experimental results. When the attachment rate of adhesion complexes is low (e.g., when adhesive parts of stripes have low adhesiveness), numerical simulations show that cells move perpendicular to substrate stripes; this striking behavior has thus far remained unobserved in experiments and merits additional numerical investigation.

Due to the complexity of the phase-field model in [28] there is no clear, simple mechanism to explain and differentiate parallel and perpendicular motions. In this work we extend the reduced model studied in [28] to a minimal model allowing for motion in any direction. In particular this model is capable of reproducing both parallel and perpendicular motion to stripes, previously only observed in the full phase-field model simulations. This minimal model suggests, in particular, the underlying mechanical processes which may give rise to perpendicular motions by elucidating the effects of biophysical (e.g., actin polymerization strength) and substrate properties (e.g., stripe sizes, adhesiveness) on the resultant direction of motion.

II. RESULTS

A. Description of the minimal model

In [28] a 2D phase-field model of cell motility was introduced to describe the onset and persistence of cell motility as well as a broad range of cell morphologies. The model contains four coupled differential equations: a phase-field equation describing the location of the cell membrane, ρ , an evolving vector field representing the actin filament network, p , a scalar equation for density of adhesion sites, A , and a Kelvin-Voigt visco-elastic equation for the deformation of the substrate, U . A description of these equations can be found in the Appendix; we omit them here for brevity.

As exploration of the full phase-field model is complicated we propose the following simplified system of differential and algebraic equations which track the location of the center of the cell (x, y) as well as the effective adhesion of the cell to the substrate A and effective substrate deformation U (see Fig. 1 for an illustration of the model):

$$\frac{d}{dt}x = V_x = f(V_x, V_y, A, y), \quad (1)$$

$$\frac{d}{dt}y = V_y = g(V_x, V_y, A, y), \quad (2)$$

$$A = A_0 \left(\frac{1}{2} (1 + \text{sign}(\sin(k_0 y))) \right) \quad (3)$$

$$\frac{d}{dt}A_0 = \bar{a}_0 - d(U)A_0 + \bar{a}_{nl}A_0^2 - \bar{s}A_0^3 \quad (4)$$

$$-\eta \frac{d}{dt}U = GU + \mu A_0. \quad (5)$$

System (1)-(5) is derived from the phase-field model in [28] after several simplifying assumptions; a detailed derivation can be found in the Appendix. Here, V_x, V_y are the velocities of the center of mass of the cell. The functions f and g are quite complex and represent the average effects of both shape deformations and the actin filaments. They are derived from the equations for the phase-field parameter ρ and the actin filaments p ; the explicit form of f and g and their derivation can be found in the Appendix.

Equation (3) encodes the striped substrate by creating inhomogeneity in the y -direction, where k_0 is the wavenumber of microprinted stripe pattern. The scalar A_0 represents the spatially homogenized number of adhesion sites (more precisely the integrin complexes which engage both substrate and the cytoskeleton). Briefly, the linear formation rate of adhesion sites is proportional to \bar{a}_0 ; due to non-linear feedback, existing adhesion sites have a tendency to form new adhesion sites with rate proportional to $\bar{a}_{nl}A^2$. Additionally there is local saturation effects represented by $\bar{s}A^3$ and coupling with U , the average substrate deformation through the $d(U)A$ term. The function

$$d(U) := \frac{1}{2} (1 + \tanh[b(U^2 - U_c^2)])$$

is an effective cut-off function which destroys adhesion sites if the substrate deformation U exceeds some critical value U_c .

The substrate is modeled as a visco-elastic material with dissipation (viscosity) η and substrate stiffness G . The substrate additionally moves in response to cell traction, represented by μA_0 .

We note that the system (4)-(5) is decoupled from equations (1)-(2) so that $A_0 = A_0(t)$ enters (1)-(2) as a time varying coefficient depending on physical parameters. Since we will focus on the effect of varying initial conditions and physical parameters on the motion of the cell, this decoupling results efficient numerical simulation. Indeed, we can compute A_0 and U independently from equations for V_x, V_y , and thus reduce overall computation time and effectively decrease the search over initial conditions by two dimensions. See Section IV for a detailed description of the numerical methods used.

Although this decoupling represents a vast simplification from the original model, subsequent numerical study

shows that we retain sufficient structure for meaningful results; future work will investigate the fully coupled system by replacing (5) by the original vector equation

$$-\eta \frac{d}{dt} \mathbf{U} = G\mathbf{U} + \mathbf{V}, \quad (6)$$

where $\mathbf{V} = (V_x, V_y)$.

In this reduced model we aim to replicate both the numerically observed emergence of perpendicular motion to the stripes as well as the experimentally observed parallel motions whereby we may study the robustness of both as well as understand the biophysical mechanisms which give rise to each.

B. Smaller driving force required for motion on striped substrate

We first consider the effect of a striped substrate on the minimal driving force required for persistent cell motion. As observed in [28] if we take \bar{a}_0 sufficiently small, e.g., $\bar{a}_0 = .0025$, then the system (4)-(5) tends to a limit cycle. On the other hand taking \bar{a}_0 large, say $\bar{a}_0 = .9$, then (4)-(5) tends to an equilibrium, suggesting the existence of a supercritical Hopf bifurcation in the parameter \bar{a}_0 ; the point of bifurcation is $\bar{a}_0 \approx .8$. For simplicity we take $\bar{a}_0 = .9$ so that the pair (A_0, U) tends to an equilibrium (A_∞, U_∞) . Following [28], we define $\kappa := 8\alpha\beta\tau_1^2 A_\infty / (81R_0^2)$, the normalized driving force in the cell and $\zeta = \tau_1 V_x / R_0$, the dimensionless velocity. In [28] a subcritical onset of motion was observed on homogeneous substrates: for $\kappa < \kappa_c \approx .746$ there is no persistent motion of the cell. At $\kappa = \kappa_c$ a fold bifurcation appears at the velocity $\zeta = 1.5$, so that for $\kappa > \kappa_c$ there are two finite velocities. Numerics suggest that the upper branch (corresponding to the larger non-zero velocity) is stable and the lower branch (corresponding to the smaller non-zero velocity) is unstable.

Upon inclusion of substrate stripes (with wavenumber $k_0 = 2.5$), the minimal driving force required for the onset of persistent motion decreases to $\kappa_c \approx .395$. As expected, this motion is parallel to the substrate stripes. A fold bifurcation appears at $\kappa = \kappa_c$ at velocity $\zeta \approx 1.6$. These numerical results are summarized in Figure 2

This predicts that microcontact printing may allow for directed cell motion even for cells which cannot sustain persistent motion on homogeneous substrates. These results are analogous to observations that the distance traveled by a motile cell is larger when restrictions to the cell geometry are imposed (e.g., diameter of the background matrix is made smaller than the cell diameter) [43]. Moreover experimental results show that microcontact printing may dominate chemical cues for contraction driven motile cells (e.g., fibroblasts) [44].

C. Robustness of vertical trajectories decreases as adhesion formation rate increases

Since $f(0, V_y, A, y) = 0$ then $V_x = 0$ is always a trivial solution of $V_x = f(V_x, V_y, A, y)$. We thus first investigate the existence of persistent motion perpendicular to the substrate pattern in the reduced system (2)-(5) with $V_x = 0$. Numerical analysis shows that persistent motion perpendicular to stripes is possible over a large range of physical parameters. For subsequent results we use parameter values in Table I unless otherwise mentioned. Estimation of these parameters is discussed in the Methods section of [28]. Values are taken to be the same as in [28], except for $\eta, \bar{a}_{nl}, \bar{s}, d$, which are modified resulting in a decrease to the period of the (A_0, U) limit cycle. These changes were necessary to achieve meaningful results and are the result of the simplifications of the model.

Surprisingly our numerical analysis also shows persistent vertical trajectories exist for all values of \bar{a}_0 (in contrast to results obtained in the full PDE model). First taking the effective linear attachment rate $\bar{a}_0 = .0025$, the A_0 - U system exhibits a limit cycle (i.e., stick-slip behavior), which in turn results in large oscillations in the y velocity, see Fig. 1. Taking $\bar{a}_0 = .9$, then the A_0 - U system tends to equilibrium but a purely perpendicular motion still exists. Oscillations in the y velocity result only from the non-homogeneity of the substrate and thus are smaller than in the case of oscillating A_0 and U_0 . Since persistent motion perpendicular to stripes is observed for all values of \bar{a}_0 , in order to corroborate our results with the full PDE simulations, we aim to understand the robustness of perpendicular trajectories via a stability analysis of the vertical motion as a function of \bar{a}_0 . That is, we consider the long time direction of motion if the initial x -velocity V_x is chosen to be non-zero. Due to the algebraic dependence of V_x in (1) classical linear stability analysis techniques are not available. Thus, to study stability of vertical trajectories, we exhaustively search initial conditions numerically in order to see long time asymptotics, for details see Section IV.

We define θ to be the angle (in degrees) of the initial velocity of the cell from the positive vertical axis, see Fig. 1. For each \bar{a}_0 we exhaustively search initial conditions y_0 in order to determine the maximal value of θ which gives rise to persistent vertical motion. We define $\max \theta$ to be the maximal θ over all possible initial conditions. The dependence of $\max \theta$ on \bar{a}_0 is shown in Fig. 3.

We observe that $\max \theta$ is largest where a_0 is small, indicating that vertical motion is more robust in this regime. This corresponds with the results in [28]; in particular $\max \theta$ is largest in the regime that the cell undergoes stick-slip motion (i.e., limit cycles in the $A_0 - U$ system). Stick-slip motion physically represents alternating phases of protrusion and retraction of the leading edge of the cell. For example, as actin filaments and adhesion sites form at the leading edge of the cell, stresses counteracting actin polymerization grow and protrude the leading edge. The adhesion sites can be thought of as many weak

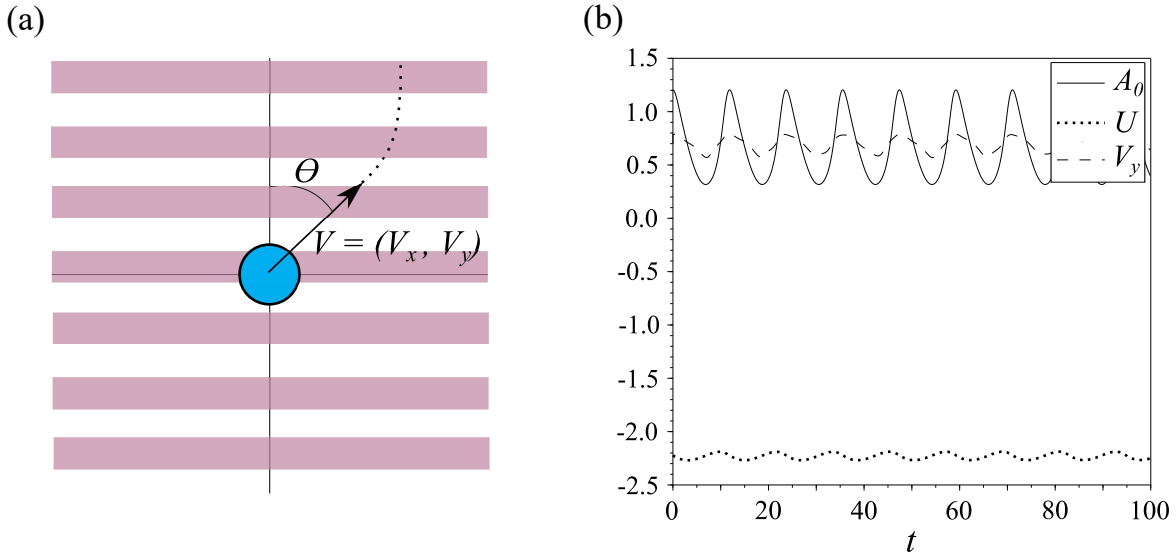


FIG. 1. (a) Sketch of cell motion on substrate with patterned stripes of adhesiveness described by (1)-(5); θ measures the deflection of the initial velocity from the vertical axis. (b) For small values of \bar{a}_0 the keratocyte experiences significant oscillations in velocity, adhesion density, and substrate deformations, here, $\bar{a}_0 = .0025$. Oscillations in number of adhesions and substrate deformations are linked to stick-slip motion. For $\bar{a}_0 > .8$, values of A_0 and U tend to a stable equilibrium. Due to inhomogeneity of the substrate, the velocity V_y still has oscillations although with smaller amplitude.

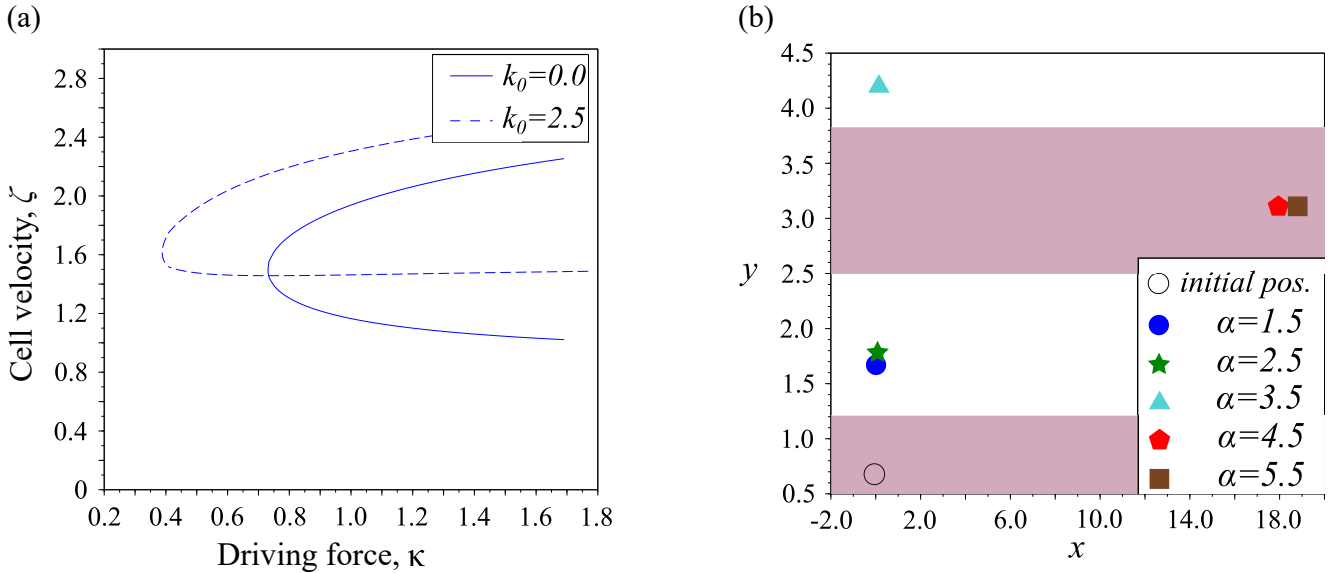


FIG. 2. (a) Bifurcation diagram showing the onset of finite velocity cell motion (with dimensionless cell velocity ζ) as the dimensionless driving force κ increases (where ζ and κ are defined in Section II B). In the absence of substrate patterns ($k_0 = 0$), the minimal driving force for the onset of motion is $\kappa_c \approx .746$ (solid line), originally calculated in [28]. In the presence of substrate patterns ($k_0 = 2.5$) the minimal driving force for cell motion decreases to $\kappa_c \approx 3.95$, providing evidence that a smaller driving force is required for motility of cells on patterned substrates. (b) The effect α on the direction of motion of the cell. The parameter α measures the rate of advection of the cell by the actin network and is a function, e.g., of the integrin ligand bond strength and actin filament stiffness. From the same initial position $(x, y) = (0, .6)$ (approximate center of an adhesive stripe) we plot the location of the cell for various values of α after simulation time $t = 25$. We take as initial velocity the solution of (1)-(2) closest to $(V_x, V_y) = (.3, .6)$. For small values of α ($\alpha < 3$) the cell halts and is trapped in a non-adhesive stripe, for moderate values of α ($3 < \alpha < 4$) the cell exhibits perpendicular motion, and for large values of α ($\alpha > 4$) the cell exhibits parallel motion. This qualitative change in behavior based on cell biophysics suggests a mechanism for cell sorting.

TABLE I. Physical parameter values used in numerical simulations.

parameter	value	description
R_0	3	radius of cell
β	3	creation of p at interface
τ_1	10	degradation of p inside cell
k_0	2.5	wave number of substrate pattern
α	1 – 3	advection of ρ by p
η	1	dissipation in the adhesive layer
G	.15	substrate stiffness
\bar{a}_0	.0025 – 1.4	linear attachment rate of adhesion sites
\bar{a}_{nl}	15	effective collective (nonlinear) attachment rate of adhesion sites
\bar{s}	10	local saturation of adhesion sites
d	10	detachment rate of adhesion sites
b	5	sharpness of breaking function
U_c	$\sqrt{5}$	critical extension to break adhesive contacts
μ	.5	effective cell/substrate traction

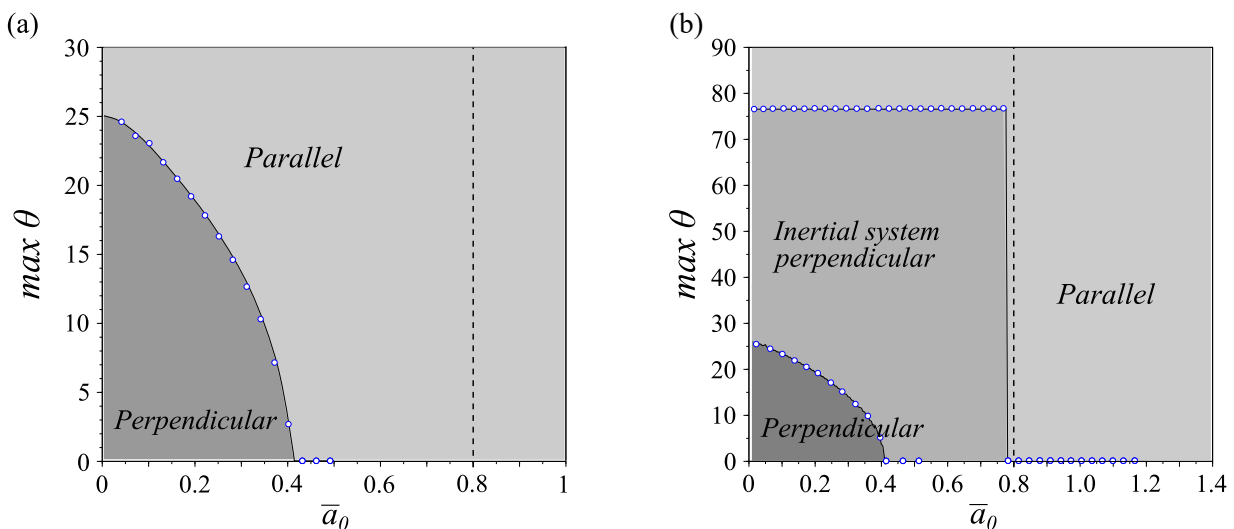


FIG. 3. (a) The maximal angle of the initial velocity for which the cell tends to persistent perpendicular motion is $\max \theta$. For small values of \bar{a}_0 perpendicular motion is possible ($\max \theta > 0$). For large values of \bar{a}_0 only parallel motion is possible. The dotted line at $\bar{a}_0 = .8$ represents the maximal value for which (A_0, U) exhibits a limit cycle; for $\bar{a}_0 < .8$ the cell exhibits stick-slip behavior (i.e., (A_0, U) exhibits a limit cycle); there the cell potentially has non-zero $\max \theta$. This provides evidence that perpendicular motion is facilitated by stick-slip behavior. Simulations are done using the system (1)-(5). (b) Simulation of (7)-(8) with (3)-(5) ($\varepsilon = .0005$) shows a larger basin of attraction for perpendicular motion. Even for nearly horizontal initial conditions the cell may eventually move perpendicular to stripes, as originally observed in the full phase-field model [28]. Dependence of $\max \theta$ on \bar{a}_0 is no longer continuous. Interestingly, the existence of perpendicular motion corresponds almost exactly to the regime of stick-slip behavior.

bonds, so that a stochastic breaking of adhesion results in a larger load of stress on the remaining adhesion sites, leading ultimately to a retraction of the leading edge.

When \bar{a}_0 is sufficiently large, the pair (A_0, U) tends to an equilibrium (A_∞, U_∞) . The equilibria A_∞ and U_∞ both increase with \bar{a}_0 . Interestingly U_∞ is approximately $U_\infty \approx R_0$ when $\max \theta = 0$. Although substrate variations of the order of magnitude of the cell size are unphysical (an artifact of our approximations), we conclude that large substrate variations may lead to stabilization of parallel motion whereas small substrate variations allow for perpendicular motion to stripes. This hypothe-

sis agrees with previous numerical and experimental evidence which shows that cells may overcome variations in substrate stiffness provided the substrate is sufficiently stiff [28, 32].

D. Aspect ratio of substrate stripes sorts cells depending on actin polymerization strength

We investigate the motion of cells on substrates with striped patterns of adhesiveness where the ratio of adhesive stripe width to non-adhesive stripe width is not

necessarily equal. Let L_1 be the width of the adhesive stripe and L_2 to be the width of the non-adhesive stripe so that $L := L_1 + L_2$ is the period of the substrate pattern. We investigate the effect of varying the ratio L_1/L on $\max\theta$.

Here, we keep \bar{a}_0 constant ($\bar{a}_0 = .0025$) and vary L_1 . Since α is a key physical parameter measuring the strength of actin polymerization, we additionally investigate how changing α changes these data. The results are summarized in Fig. 4.

It is clear that if $L_1 = 0$ or $L_1 = L$ then the cell cannot create a biased directionality and $\max\theta = 0$. This is expected since if the adhesive stripe is too small then the cell cannot develop a sufficient number of adhesive bonds to the substrate to initiate persistent motion. On the other hand if $L_1/L \approx 1$ the substrate is entirely adhesive and the substrate is effectively homogeneous.

Interestingly we observe an inverse, monotonic dependence between the actin polymerization strength α and the percentage of adhesiveness of the substrate which results in perpendicular motion to stripes. If the substrate is predominantly non-adhesive then the cell requires high actin polymerization strength to generate perpendicular motion and vice-versa. This suggests that different effectiveness of internal biophysical parameters may lead to different behaviors of the cell depending on the shape of the patterned substrate, providing evidence for cell sorting and directed cell motility. In Figure 2 we plot the location of cells with varying values of α after simulation time $t = 25$. We initialize all cells at location $(x, y) = (0, .6)$, which is in the middle of an adhesive stripe of the substrate. For comparison, we take as initial velocity for each cell the solution of (1)-(2) closest to $(V_x, V_y) = (.3, .6)$. We observe that for small values of α ($\alpha < 3$) the cell halts on the non-adhesive stripe. Additionally, for moderate values of α ($3 < \alpha < 4$) the cell exhibits perpendicular motion, while for large values of α ($\alpha > 4$) the cell exhibits parallel motion to stripes.

E. Inertia increases the basin of attraction of persistent perpendicular motion

Thus far, the basin of attraction for vertical motion has been bounded by $\max\theta < 40$. However in full PDE simulations even with motion initialized parallel to the stripes, the cell switches directions and begin moving perpendicular to the stripes (provided a_0 is sufficiently small) so that $\max\theta \approx 90$. We predict that this discrepancy arises from the lack of memory in the reduction (1) - (5). That is, we neglect both shape deformation and directional inertia (or memory) which are present in the full PDE model. In particular, there is finite time relaxation of the actin vector field which is neglected in the reduced equations.

To include these inertial effects we modify (1)-(2):

$$\varepsilon \ddot{x} + \dot{x} = f(\dot{x}, \dot{y}, A, y) \quad (7)$$

$$\varepsilon \ddot{y} + \dot{y} = g(\dot{x}, \dot{y}, A, y), \quad (8)$$

where ε is an effective inertial coefficient characterizing the time of relaxation of the cell's directional inertia. This coefficient is a function of both shape deformations and relaxation of the actin polymerization field. Mathematically it is also important to note that $\varepsilon > 0$ provides regularization in (7)-(8) absent in (1)-(2), e.g., given initial conditions, solutions are now unique for all time. We compare numerical results with those results obtained for $\varepsilon = 0$, see Fig. 4. Again, our interest is to study the dependence on $\max\theta$ as a function of \bar{a}_0 .

As (7)-(8) is a singular perturbation of (1)-(2), it is natural that the behavior drastically changes qualitatively. However, it is surprising that the value of $\max\theta$ becomes approximately piecewise constant in numerical studies. We observe that for $\varepsilon = .0005$ the positive value of $\max\theta$ is very large: $\max\theta \approx 77$, agreeing with simulations in [28]. This suggests that memory of shape deformations as well as persistence of the actin network may be correlated with persistent motion perpendicular to the stripes. **Moreover we note that by varying the value of ε over two orders of magnitude ($\varepsilon = 0.0001$ to $\varepsilon = 0.01$), the effect on values of $\max\theta$ is very small, so we omit these results.**

III. DISCUSSIONS

We have presented a reduced system derived from the full phase-field model of [28]. The reduced system is much less computationally expensive to solve while still retaining meaningful qualitative solutions: we reproduce both perpendicular and parallel persistent cell motions on periodically striped substrates. Our numerical study indicates that the robustness of vertical and horizontal motions can be quantified via consideration of long time asymptotics over all initial conditions (measured by $\max\theta$). These simulations indicate that small adhesion site formation rates are necessary for persistence of perpendicular motions.

Moreover, we observed an inverse, monotonic dependence of actin polymerization strength on the amount of adhesive substrate which would lead to perpendicular motions. We believe that carefully engineered substrates could utilize this relationship in applications of cell sorting and directed cell motility. We interpret the inverse dependence of actin polymerization strength and substrate adhesion on the ability to move perpendicular to stripes physically as follows. The actin polymerization strength and substrate adhesion together generate traction forces of the cell on the substrate. So, our results indicate that if the traction forces generated by the cell on the substrate are too large, then the cell cannot achieve perpendicular motion to stripes. On the other

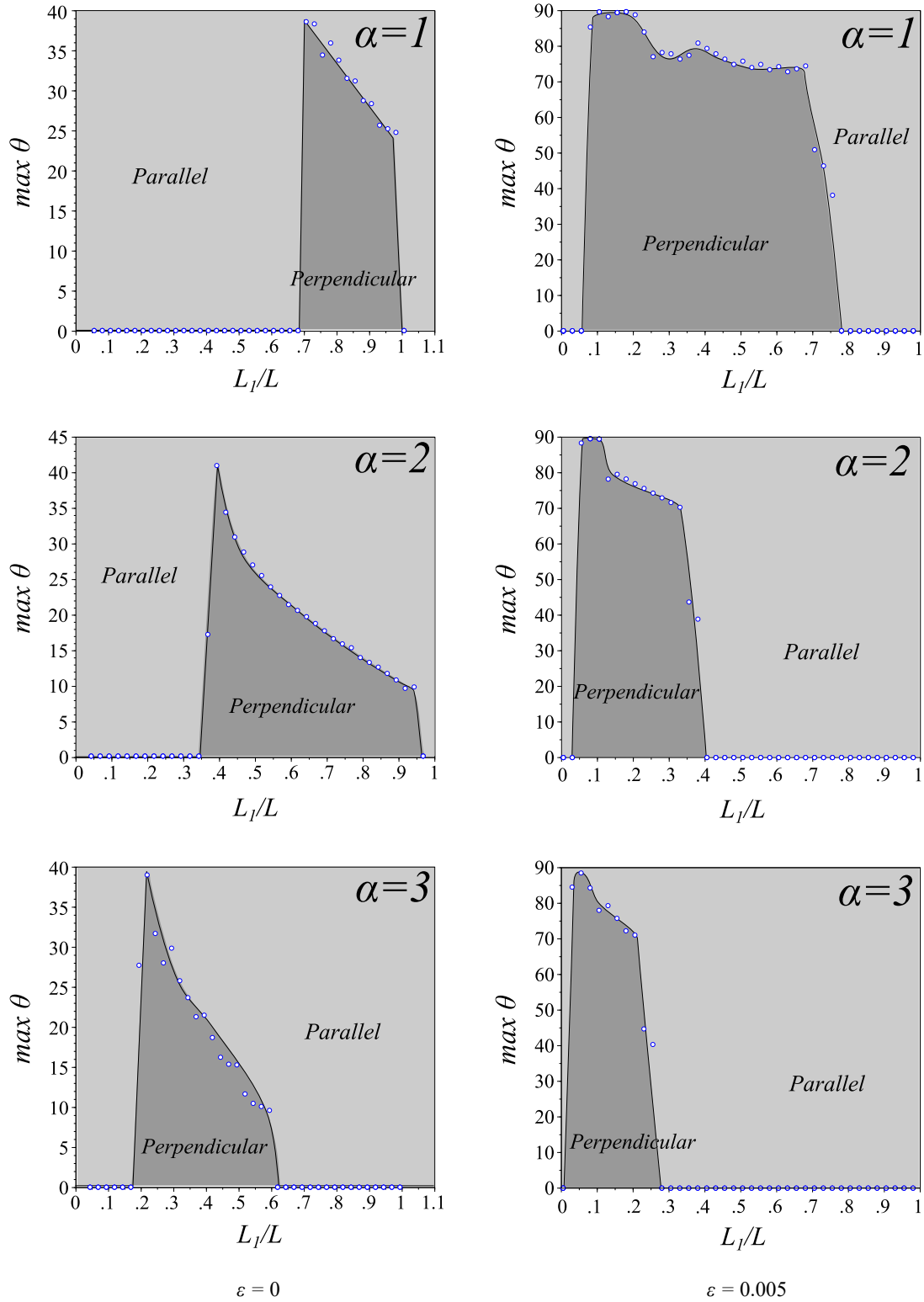


FIG. 4. The value of α and substrate pattern affect the direction of keratocyte motion. The value of α measures the rate of advection of the cell by the actin network. The patterned substrate has constant period L but has varying width L_1 of the adhesive stripe. It is seen that if α is small then the cell requires a wider adhesive stripe in order to move perpendicular to the stripe and vice versa. This suggests a mechanism for cell guiding and sorting. These trends hold both for dynamics with and without inertia. For all simulations we fix $\bar{a}_0 = .0025$. For simulations with inertia we use $\varepsilon = 0.005$.

hand, if the generated traction forces are small (but still large enough to generate persistent motion), then the cell may move perpendicular to stripes.

Further developing this physical mechanism, one can imagine a cell which is initially moving perpendicular to stripes. If the substrate adhesion bonds are too strong, then the cell is “pulled” towards the adhesive parts of the substrate, preventing the cell from crossing non-adhesive stripes. On the other hand, if substrate adhesion bonds are relatively weak, then the directional inertia of the actin network may overcome those forces which are “pulling” the cell towards adhesive regions so that the cell crosses the non-adhesive stripe and achieves perpendicular motion.

Finally, by including memory (e.g. due to a finite relaxation time of the cell shape) we obtain a singularly perturbed system which shows closer agreement with full phase-field simulations: for small values of \bar{a}_0 the initial velocity may be almost parallel to stripes and still we observe persistent perpendicular motion over long time. These results suggest that shape deformation and directional inertia of the cell are necessary for the cell to move perpendicular to the substrate stripes in a robust way.

We believe that this methodology of reduction from a PDE model to finite dimensional models (e.g., systems of ordinary differential equations) may be applicable to a wide range of physical models. Their subsequent analytical and numerical study may provide new physical insights.

IV. METHODS

We solve system (1) - (5) using a forward Euler finite difference scheme, resulting in an explicit scheme for both A_0 and U . For example, $A_0^{t+\Delta t}$, the value of A_0 at time $t + \Delta t$, depends only on the values of the previous time steps:

$$A_0^{t+\Delta t} = A_0^t + \Delta t [\bar{a}_0 - d(U^t)A_0^t + \bar{a}_{nl}(A_0^t)^2 - \bar{s}(A_0^t)^3]. \quad (9)$$

We note that V_x is defined via an algebraic equation, as opposed to a differential equation. As such, to solve the implicitly defined velocities V_x and V_y we first require a nonlinear function solver. We use a predefined function in Scilab (fsolve), which is based on an iterative Powell hybrid method and again use a forward Euler finite difference scheme to update $(x^{t+\Delta t}, y^{t+\Delta t})$, the position of the cell at time $t + \Delta t$, based on the velocity at time t , (V_x^t, V_y^t) :

$$x^{t+\Delta t} = x^t + \Delta t V_x^t \quad (10)$$

$$y^{t+\Delta t} = y^t + \Delta t V_y^t. \quad (11)$$

We verified the validity of the numerical scheme by taking sufficiently small time discretizations until the numerical solutions converged.

In order to conduct an exhaustive search through all initial conditions we first simulate the longtime dynamics

of (4)-(5) to determine either the value of the equilibrium point or the stable limit cycle. In the former case, we assign the limiting equilibrium value as the initial conditions for A_0 and U . In the latter case, we fix a point on the limit cycle. For consistency, we choose the point on the limit cycle where A_0 is maximal. Simulations indicate that fixing this initial condition for (A_0, U) is qualitatively the same as simulation of all initial conditions for (A_0, U) on its limit cycle.

When viewed as an algebraic system, (1)-(2) has non-unique solutions (V_x, V_y) for fixed y . Thus for a fixed value of $y_0 \in [0, k_0/2\pi]$ we compute all admissible initial velocities $V_x(0), V_y(0)$ and simulate the long time dynamics of each. We note that since solutions of (1)-(2) will generically be non-unique, to ensure physical solutions we assume that velocities are continuously changing in time; that is we initialize the iterative solver at the velocity of the previous time step. This provides a type of inertia which we distinguish from that introduced in (7)-(8): indeed continuity of velocity captures inertia which is present even in the absence of actin dynamics and shape deformations. System (7)-(8) reincorporates the inertia of the actin filaments and shape deformations of the cell, which are originally lost in the minimal approximation.

For each numerical solution we deduce if either (i) the motion becomes eventually horizontal, (ii) the motion becomes eventually vertical, (iii) the motion eventually stops, or (iv) there is no continuous in time velocity which solves (1)-(2) for all time. Since the equations (1)-(2) are nonlinearly coupled, case (iii) may arise, for example, as the result of bifurcations in the V_x - V_y solution plane as A or y vary. If such a discontinuity occurs, it is deemed unphysical and so we omit this scenario from our analysis. We believe that these unphysical results are due to the decoupling of the (A_0, U) dynamics from the (V_x, V_y) dynamics, which may lead to “out-of-phase” oscillations of the (A_0, U) and (V_x, V_y) systems. We expect that recoupling their dynamics (e.g., by replacing (5) by (6)) may remove these unphysical behaviors; this is left for future work.

Thus, a summary of our numerical algorithm to solve (1)-(5) is

1. Fix physical parameter values
2. Initialize the values (A_0, U) to correspond to either the maximal A_0 value of the limit cycle or the equilibrium value.
3. For all initial positions $y \in [0, k_0/2\pi]$ and all initial velocities (which solve (1)-(2)), calculate the long time behavior of the velocity (V_x, V_y) .

To solve the system with inertia, (7)-(8), we only change the method by which we solve for (V_x, V_y) . Here, let $(S, T) = (V_x, V_y)$ so that

$$\varepsilon \dot{S} + S = f(S, T, A, y) \quad (12)$$

$$\varepsilon \dot{T} + T = g(S, T, A, y) \quad (13)$$

constitutes a system of first order differential equations (with known parameter y). Then, as above we use a forward Euler finite difference scheme to solve for S, T in terms of the values at previous time steps. We note that solving (7)-(8) requires small time steps $\Delta t \ll \varepsilon$ to ensure convergence as it is a singularly perturbed system.

In general we may take any initial velocities $V_x(0), V_y(0)$, however we restrict ourselves to initial conditions which are compatible with initial velocities computed in the case that $\varepsilon = 0$ so that results may be compared: given an initial y_0 we initialize $V_x(0), V_y(0)$ to be admissible solutions to the system (1)-(2).

-
- [1] Mohan, R. R. et al. Apoptosis, necrosis, proliferation, and myofibroblast generation in the stroma following LASIK and PRK. *Exp. Eye. Res.* **76**, 7187 (2003).
- [2] Banchereau, J. & Steinman, R. M. Dendritic cells and the control of immunity. *Nat.* **392**, 245252 (1998).
- [3] Birchmeier, C., Birchmeier, W., Gherardi, E. & Woude, G. F. V. Met, metastasis, motility and more. *Nat. reviews Mol. cell biology* **4**, 915925 (2003).
- [4] Pollard, T. D. The cytoskeleton, cellular motility and the reductionist agenda. *Nat.* **422**, 741745 (2003).
- [5] Pollard, T. D. & Borisy, G. G. Cellular motility driven by assembly and disassembly of actin filaments. *Cell* **112**, 453465 (2003).
- [6] Barnhart, E. L., Lee, K., Keren, K., Mogilner, A. & Theriot, J. A. An adhesion-dependent switch between mechanisms that determine motile cell shape. *PLoS Biol* **9**, e1001059 (2011).
- [7] Abercrombie, M. The crawling movement of metazoan cells. *Proc R Soc Lond. B* **207.1167**, 129147 (1980).
- [8] Sheetz, M. P., Felsenfeld, D. P. & Galbraith, C. G. Cell migration: regulation of force on extracellular-matrix-integrin complexes. *Trends cell biology* **8**, 5154 (1998).
- [9] Keren, K. et al. Mechanism of shape determination in motile cells. *Nat.* **453**, 475480 (2008).
- [10] Verkhovskiy, A. B., Svitkina, T. M. & Borisy, G. G. Self-polarization and directional motility of cytoplasm. *Curr. Biol.* **9**, 11S1 (1999).
- [11] Mogilner, A. & Odde, D. Modeling cellular processes in 3d. *Trends cell biology* **21**, 692700 (2011).
- [12] Mogilner, A. Mathematics of cell motility: have we got its number? *J. Math. Biol.* **58**, 105134 (2009).
- [13] Camley, B. A., Zhao, Y., Li, B., Levine, H. & Rappel, W.-J. Crawling and turning in a minimal reaction-diffusion cell motility model: coupling cell shape and biochemistry. *Phys. Rev. E* **95**, 012401 (2017).
- [14] Ziebert, F., Swaminathan, S. & Aranson, I. S. Model for self-polarization and motility of keratocyte fragments. *J. The Royal Soc. Interface* rsif20110433 (2011).
- [15] Recho, P., Putelat, T. & Truskinovsky, L. Contraction-driven cell motility. *Phys. review letters* **111**, 108102 (2013).
- [16] Rubinstein, B., Jacobson, K. & Mogilner, A. Multiscale two-dimensional modeling of a motile simple-shaped cell. *Multiscale Model. & Simul.* **3**, 413439 (2005).
- [17] Shao, D., Rappel, W. J. & Levine, H. Computational model for cell morphodynamics. *Phys. Rev. Lett.* **105**, 108104 (2010).
- [18] Tjhung, E., Tiribocchi, A., Marenduzzo, D. & Cates, M. E. A minimal physical model captures the shapes of crawling cells. *Nat. communications* **6** (2015).
- [19] Löber, J., Ziebert, F. & Aranson, I. S. Collisions of deformable cells lead to collective migration. *Sci. reports* **5**, 9172 (2015).
- [20] Ziebert, F. & Aranson, I. S. Computational approaches to substrate-based cell motility. *npj Comput. Mater.* **2**, 16019 (2016).
- [21] Berlyand, L., Potomkin, M. & Rybalko, V. Non-uniqueness in a nonlinear sharp interface model of cell motility. *Comptes Rendus Math.* **354(10)**, 986992 (2016).
- [22] Mizuhara, M. S., Berlyand, L., Rybalko, V. & Zhang, L. On an evolution equation in a cell motility model. *Phys. D: Nonlinear Phenom.* **318**, 1225 (2016).
- [23] Mizuhara, M. S. & Zhang, P. Uniqueness and traveling waves in a cell motility model. *arXiv:1703.00811* (2017).
- [24] Recho, P. & Truskinovsky, L. Cell locomotion in one dimension. In *Physical Models of Cell Motility*, 135197 (Springer, 2016).
- [25] Barnhart, E., Lee, K.-C., Allen, G. M., Theriot, J. A. & Mogilner, A. Balance between cell-substrate adhesion and myosin contraction determines the frequency of motility initiation in fish keratocytes. *Proc. Natl. Acad. Sci.* **112**, 50455050 (2015).
- [26] Barnhart, E. L., Allen, G. M., Jülicher, F. & Theriot, J. A. Bipedal locomotion in crawling cells. *Biophys. journal* **98**, 933942 (2010).
- [27] Löber, J., Ziebert, F. & Aranson, I. S. Modeling crawling cell movement on soft engineered substrates. *Soft matter* **10**, 13651373 (2014).
- [28] Ziebert, F. & Aranson, I. S. Effects of adhesion dynamics and substrate compliance on the shape and motility of crawling cells. *PLoS ONE* **8**, e64511 (2013).
- [29] Csucs, G., Quirin, K. & Danuser, G. Locomotion of fish epidermal keratocytes on spatially selective adhesion patterns. *Cell motility cytoskeleton* **64**, 856867 (2007).
- [30] Doyle, A. D., et al. One-dimensional topography underlies three-dimensional fibrillar cell migration. *The Journal of cell biology* **184.4**, 481-490 (2009).
- [31] Ramirez-San Juan, G. R., Oakes, P. W. & Gardel, M. L.. Contact guidance requires spatial control of leading-edge protrusion. *Molecular Biology of the Cell* **28.8**, 1043-1053 (2017).
- [32] Rolli, C. G. et al. Switchable adhesive substrates: revealing geometry dependence in collective cell behavior. *Biomater.* **33**, 24092418 (2012).
- [33] Chen, C. S., Mrksich, M., Huang, S., Whitesides, G. M. & Ingber, D. E. Micropatterned surfaces for control of cell shape, position, and function. *Biotechnol. progress* **14**, 356363 (1998).
- [34] Albert, P. J. & Ulrich S. Schwarz. Optimizing micropattern geometries for cell shape and migration with genetic algorithms. *Integrative Biology* **8.7**, 741-750 (2016).
- [35] Lo, C.-M., Wang, H.-B., Dembo, M. & Wang, Y.-L. Cell movement is guided by the rigidity of the substrate. *Biophys. journal* **79**, 144152 (2000).
- [36] Trichet, L. et al. Evidence of a large-scale mechanosens-

- ing mechanism for cellular adaptation to substrate stiffness. *Proc. Natl. Acad. Sci.* **109**, 69336938 (2012).
- [37] Mahmud, G., et al. Directing cell motions on micropatterned ratchets. *Nature physics* **5.8**, 606-612 (2009).
- [38] Shekaran, A. & Garcia, A. J. Nanoscale engineering of extracellular matrix-mimetic bioadhesive surfaces and implants for tissue engineering. *Biochimica et Biophys. Acta (BBA)-General Subj.* **1810**, 350360 (2011).
- [39] Bruinsma, R., Goulian, M. & Pincus, P. Self-assembly of membrane junctions. *Biophys. journal* **67**, 746750 (1994).
- [40] Burridge, K. & Chrzanowska-Wodnicka, M. Focal adhesions, contractility, and signaling. *Annu. review cell developmental biology* **12**, 463519 (1996).
- [41] Sackmann, E. & Bruinsma, R. F. Cell adhesion as wetting transition? *ChemPhysChem* **3**, 262269 (2002).
- [42] Smith, A.-S. & Seifert, U. Effective adhesion strength of specifically bound vesicles. *Phys. Rev. E* **71**, 061902 (2005).
- [43] Peyton, S. R. et al. Marrow-derived stem cell motility in 3d synthetic scaffold is governed by geometry along with adhesivity and stiffness. *Biotechnol. bioengineering* **108**, 11811193 (2011).
- [44] Rodriguez, L. L. & Schneider, I. C. Directed cell migration in multi-cue environments. *Integr. Biol.* **5**, 13061323 (2013).

V. APPENDIX

A. Phase-field model

In [14] a 2D phase-field model of cell motility was introduced to describe the onset and persistence of cell motility as well as a broad range of cell morphologies. This model contains two PDEs. First, a phase-field parameter ρ describes the location of the cell membrane (i.e., $\rho \approx 1$ on the interior of the cell and $\rho \approx 0$ outside of the cell). Second, the motion of the cell membrane is actively driven by a vector field p which models the averaged orientation field of the actin filament network.

The coupling of these equations reflects two main experimental observations: (i) the nucleation of branches of actin filaments near the cell membrane via Wiskott-Aldrich syndrome proteins (WASP) activation of the ARP2/3 complex and (ii) presence of actin filaments allows for the creation of adhesive contacts and subsequent transfer of momentum of the polymerizing actin network to the substrate driving the cell membrane. Additionally the model enforces approximate volume preservation. The full PDE model introduced in [14] is:

$$\partial_t \rho = D_\rho \Delta \rho - (1 - \rho)(\delta - \rho)\rho - \alpha A p \cdot (\nabla \rho), \quad (14)$$

$$\partial_t p = -\tau_1^{-1} p - \tau_2^{-1} (1 - \rho^2) p - \beta \nabla \rho - \gamma [(\nabla \rho) \cdot p] p. \quad (15)$$

Volume preservation of the cell is enforced by introducing a time-dependence in the double-well potential of the phase-field model via $\delta = \delta(t)$ (for details, see [14]):

$$\delta(t) := \frac{1}{2} + \mu \left(\int \rho(x, y, t) dx dy - V_0 \right), \quad (16)$$

with μ the stiffness of the volume preservation constraint. Integration here and in all subsequent calculations is taken over the 2D plane. For our subsequent analysis we assume that $\tau_2^{-1} = \gamma = 0$. In particular, the term containing γ accounts for symmetry breaking due to myosin driven contraction in the rear of the cell; since our subsequent analysis initializes data with non-zero velocities, this symmetry breaking is not required for capturing persistent motion. Moreover it is mentioned in [28] that self-sustained cell motion is possible in the system (14)-(15) even without this term. We refer the interested reader to [14, 28] for a full description of the model.

In [14] it is assumed for simplicity that the friction generated from adhesion complexes is homogeneous so that A is constant. To account for the complex interaction between cell and substrate it is necessary to include the dynamics of adhesion site formation, see [28]:

$$\partial_t A = D_A \Delta A + \rho(a_0 p^2 + a_{nl} A^2) - s A^3 - d(U) A. \quad (17)$$

These adhesion contacts describe integrin complexes which (through a series of intermediate proteins such as zyxin, talin, and vinculin) engage both the substrate and the cytoskeleton.

In the final term of (17), the function $d(U)$ describes the coupling of A to the average substrate deformation $\mathbf{U}(t)$, with $U = |\mathbf{U}|$:

$$d(U) = \frac{1}{2} (1 + \tanh[b(U^2 - U_c^2)]), \quad (18)$$

where \mathbf{U} satisfies

$$\frac{d}{dt} \mathbf{U} = -\frac{1}{\eta} (G \mathbf{U} + \mathbf{V}), \quad (19)$$

where η is the effective viscous friction of the substrate, G is an effective spring constant and \mathbf{V} is the velocity of the cell's center of mass. That is, the substrate is viewed as a Kelvin-Voigt visco-elastic material and adhesion sites are broken if deformations exceed the threshold U_c .

As all attachment/detachment rates are effective parameters, they incorporate both characteristics of the adhesion complex as well as the substrate preparation. Thus, spatial inhomogeneity in the substrate may be introduced through coefficients, e.g., spatial dependence of $a_0 = a_0(y)$.

B. Derivation of the reduced system

We reduce the system (14) to a two-dimensional system for the location of the center of the cell (x, y) . All assumptions are analogous to those made in [28]. The biggest difference is that we do not assume that $V_y \ll 1$ and as such we have more complex coupling between all equations. We first assume that the cell has fixed circular shape for all time:

$$\rho(x, y, t) = \rho(x - x_0(t), y - y_0(t)), \quad (20)$$

where

$$\rho(x, y) = \exp(-(x^2 + y^2)/R_0^2). \quad (21)$$

In particular, using ansatz (20) and definition (16), we see that the total area enclosed by the cell is fixed and that $\delta \equiv \frac{1}{2}$. We denote the velocity of the center of the cell $V = (V_x, V_y) = (\dot{x}_0, \dot{y}_0)$. Multiplying (14) by $\partial_x \rho$, and integrating over the domain yields

$$V_x \int (\partial_x \rho)^2 = \alpha \int A p \cdot (\nabla \rho) \partial_x \rho. \quad (22)$$

Likewise multiplying (14) by $\partial_y \rho$ and integrating we have

$$V_y \int (\partial_y \rho)^2 = \alpha \int A p \cdot (\nabla \rho) \partial_y \rho. \quad (23)$$

We likewise assume that

$$p(x, y, t) = p(x - x_0(t), y - y_0(t)) \quad (24)$$

to rewrite equation (15):

$$-V \cdot \nabla p = -\tau_1^{-1} p - \beta \nabla \rho. \quad (25)$$

Under the assumption that $|V|$ is small:

$$p(x - \tau_1 V_x, y - \tau_1 V_y) = p - \tau_1 V \cdot \nabla p + O(\tau_1^2 V^2) \quad (26)$$

$$= -\tau_1 \beta \nabla \rho(x, y). \quad (27)$$

Thus to first order

$$p(x, y) = -\tau_1 \beta \nabla \rho(x + \tau_1 V_x, y + \tau_1 V_y). \quad (28)$$

To simplify the equation for A we first consider the problem on a homogeneous substrate (i.e., a_0 is constant) and consider the following ansatz for the adhesion sites density: $A = A_0(t)\rho(x, y, t) + \delta A_1(x, y, t)$ where δ is much smaller than the size of the cell. That is, we assume that A is essentially spatially constant on the interior of the cell. Plugging this expansion into (17) and integrating over the domain we have to leading order:

$$\frac{d}{dt} A_0 = \bar{a}_0 - d(U) A_0 + \bar{a}_{nl} A_0^2 - \bar{s} A_0^3, \quad (29)$$

where

$$\bar{a}_0 = a_0 \frac{\langle \rho \rho^2 \rangle}{\langle \rho \rangle}, \bar{a}_{nl} = a_{nl} \frac{\langle \rho^3 \rangle}{\langle \rho \rangle}, \bar{s} = s \frac{\langle \rho^3 \rangle}{\langle \rho \rangle}, \quad (30)$$

with $\langle f \rangle := \int f dx dy$.

Similarly we can simplify the equation for \mathbf{U} to a scalar equation under the assumption that U and V are essentially co-linear. As in [28] we make the approximation $V(t) \approx \langle \alpha A_0 p \rangle \approx \bar{\alpha} A_0$, where μ is a numerical constant:

$$-\eta \partial_t U = GU + \mu A_0. \quad (31)$$

We note that the assumption $V(t) \approx \bar{\alpha} A_0$ decouples the $A_0 - U$ system from the $V_x - V_y$ system. This is

a restrictive assumption, which we alternatively motivate as follows: the equation for substrate deformation is $\eta \frac{d}{dt} U = GU + V$. Writing the equation for velocity in the form $V = F(A_0, y)$, we have after substitution $\eta \frac{d}{dt} U = GU + F(A_0, y)$. Averaging with respect to the y -variable (e.g., when the substrate period is fast compared to the limit cycle period), then the equation is written $\eta \frac{d}{dt} U = GU + \bar{F}(A_0)$, decoupling the systems.

Finally, in order to simulate the patterned substrate we approximate A to have the form

$$A = A_0(t) \left(\frac{1}{2} (1 + \text{sign}(\sin(k_0 y))) \right). \quad (32)$$

For subsequent numerical simulations, we use the first two terms of the Fourier expansion of (32) for simplicity and regularity.

By plugging in (28), (32) into (22)-(23), we derive the equations $V_x = f(V_x, V_y, A, y)$, $V_y = g(V_x, V_y, A, y)$, where f and g are defined as follows:

$$f := I_0 \cdot (I_1 - 6e^{-(1/12)k_0^2 R_0^2} (I_2 + I_3) - 2e^{-(3/4)k_0^2 R_0^2} (I_4 + I_5))$$

where

$$I_0 := \left(\frac{4\alpha A \beta}{243\pi R_0^4} \right) e^{-(2\tau_1^2(V_x^2 + V_y^2))/(3R_0^2)} \tau_1^2 V_x$$

$$I_1 := 3\pi (-3R_0^2 + 4\tau_1^2(V_x^2 + V_y^2))$$

$$I_2 := 2k_0 R_0^2 \tau_1 V_y \cos(k_0((\tau_1 V_y)/3 + y_0))$$

$$I_3 := (-6R_0^2 + k_0^2 R_0^4 + 8\tau_1^2(V_x^2 + V_y^2)) \cdot \sin(k_0((\tau_1 V_y)/3 + y_0))$$

$$I_4 := 6k_0 R_0^2 \tau_1 V_y \cos(k_0(\tau_1 V_y + 3y_0))$$

$$I_5 := (-6R_0^2 + 9k_0^2 R_0^4 + 8\tau_1^2(V_x^2 + V_y^2)) \cdot \sin(k_0(\tau_1 V_y + 3y_0)),$$

and

$$g := J_0 \cdot (J_1 \cdot J_2 + J_3 + \tau_1 V_y (-3R_0^2 + 4\tau_1^2(V_x^2 + V_y^2))(J_4 + J_5)).$$

where

$$J_0 := - \left(\frac{4\alpha A \beta}{243\pi R_0^4} \right) e^{-(3/4)k_0^2 R_0^2 - (2\tau_1^2(V_x^2 + V_y^2))/(3R_0^2)} \tau_1$$

$$J_1 := -24R_0^2 + k_0^2 R_0^4 + 4\tau_1^2(2V_x^2 + 3V_y^2)$$

$$J_2 := 3e^{(2k_0^2 R_0^2)/3} k_0 R_0^2 \cos(k_0((\tau_1 V_y)/3 + y_0))$$

$$J_3 := 3k_0 R_0^2 (-24R_0^2 + 9k_0^2 R_0^4 + 4\tau_1^2(2V_x^2 + 3V_y^2)) \cdot \cos(k_0(\tau_1 V_y + 3y_0))$$

$$J_4 := -3\pi e^{(3k_0^2 R_0^2)/4} + 12e^{(2k_0^2 R_0^2)/3} \cdot \sin(k_0((\tau_1 V_y)/3 + y_0))$$

$$J_5 := 4 \sin(k_0(\tau_1 V_y + 3y_0))$$

For all simulations we use parameter values from Table I.

If we assume that $V_y = 0$ we of course recover equation (14) in [28]. We note that due to homogeneity of the substrate in the x direction, equation $V_x = f(V_x, V_y, A, y)$ is algebraic; letting $\zeta = V_x$:

$$\zeta = f(\zeta, \dot{y}, y) \quad (33)$$

$$\dot{y} = g(\zeta, \dot{y}, y). \quad (34)$$

Importantly (33)-(34) may not be in general solvable (or have a continuous in time solution) for all values of \dot{y}, y . This leads to difficulty of both numerical simulations as well as prevents the use of classical linear stability analysis.

We highlight here that the reduction described above is similar to the one conducted in [28] however we addition-

ally incorporate expansions for the V_y component. Moreover the equation for the effective adhesion A_0 is derived using the asymptotic expansion $A = A_0(t)\rho(x, y, t) + \delta A_1(x, y, t)$ which gives rise to the effective coefficients (30).

ACKNOWLEDGMENTS

The work of M.S.M. and L.B. was supported by NSF grant DMS-1405769. In addition M.S.M. was supported by the Department of Defense (DoD) through the National Defense Science & Engineering Graduate Fellowship (NDSEG) Program. The research of I.S.A. was supported by the US Department of Energy (DOE), Office of Science, Basic Energy Sciences (BES), Materials Science and Engineering Division.